IEEE Access
Multidisciplinary | Rapid Review | Open Access Journal

Received July 29, 2020, accepted August 10, 2020, date of publication August 14, 2020, date of current version August 25, 2020.

Digital Object Identifier 10.1109/ACCESS.2020.3016740

EMD-Based Borehole TEM Array Signal Denoising and Baseline Wander Correction for NDT of Downhole Casings

BO DANG[1], CHANGZAN LIU[2], LING YANG[1], GANG WANG[1], MIMI WANG[1], ZHIPING REN[1], (Member, IEEE), AND RUIRONG DANG[1]

[1]Shaanxi Key Laboratory of Measurement and Control Technology for Oil and Gas Wells, Xi'an Shiyou University, Xi'an 710065, China
[2]School of Marine Science and Technology, Northwestern Polytechnical University, Xi'an 710072, China

Corresponding author: Bo Dang (bodang521@126.com)

This work was supported in part by the National Science and Technology Major Project under Grant 2016ZX05028-001, in part by the National Natural Science Foundation of China under Grant 51974250 and Grant 41874158, in part by the Youth Science and Technology Nova Project in Shaanxi Province, China, under Grant 2020KJXX-018, in part by the Natural Science Basic Research Plan in Shaanxi Province of China under Grant 2018JQ5133, and in part by the Natural Science Foundation of Shaanxi Province Department of Education under Grant 17JS106.

ABSTRACT Transient electromagnetic (TEM) techniques have been proven to be efficient for nondestructive testing (NDT) operations due to their pulsed eddy-current properties. However, in the field of downhole measurements, harsh environments may significantly influence the NDT performance in downhole casings. In this paper, an empirical mode decomposition (EMD) method based on borehole TEM array signal denoising and baseline wander (BW) correction is proposed to compensate for the bad measurement conditions that affect downhole NDT. Based on the borehole TEM signal model, we investigated the principle of the EMD approach for the borehole TEM response, where the background magnetic noise and temperature drift effects were analyzed by considering the motion measurement and effective permeability. It was found out that although the BW can be effectively removed with the EMD approach, the performance of the signal denoising is closely related to the measurement speed of the downhole NDT sensors. To solve this problem, we proposed an array-based ensemble EMD method to improve the denoising performance of the borehole TEM signals by formulating a three-dimensional borehole TEM data structure, where the generation of the noise-aided data can be more efficient by employing the borehole TEM array. The performance of the proposed method was verified by applying it to a borehole TEM system for the NDTs of oil-well casings. In addition, field experiments were conducted, and the results demonstrated the effectiveness of the proposed method.

INDEX TERMS Borehole, transient electromagnetic system, array, nondestructive testing, empirical mode decomposition.

I. INTRODUCTION

Borehole transient electromagnetic (TEM) [1] techniques are widely used in the field of the nondestructive testing (NDT) of downhole metal casings [2], [3] due to their rapid and accurate acquisition of broad-frequency-range data [4], [5], pulsed eddy-current properties [6], [7], and accessibility to targets [8]. However, the harsh environments of bad borehole conditions, such as the narrow underground confined space [9], cumbersome metal tool housings against the high wellbore pressure [10], high temperatures [11], and required motion measurements for improving the measurement efficiency [12], making borehole TEM systems quite different from those used for surface measurements. Thus, such environments have a great influence on the performance of NDTs in downhole casings.

To overcome the impacts of the bad borehole conditions, a lot of research works have been conducted with respect to the design and use of eddy-current sensors for improving the performance of downhole NDTs. Aimed at improving the signal-to-noise ratio (SNR) of borehole TEM systems, multi-turn approaches [13]–[16] that are composed of coaxial

The associate editor coordinating the review of this manuscript and approving it for publication was Naveed Ur Rehman.

multi-turn transmitting and receiving coils wound around magnetic or air cores were proposed to enhance the eddy-current response in high-temperature applications. Based on the correlation of the multiple receivers with the different distances between the transmitting and receiving (TRD) coils [13], [14], a multi-receive single transmit TEM array was proposed to improve the SNR of borehole TEM systems for NDTs in downhole casings, and the multi-receive array was weighted according to the array signal processing in order to improve the detection performance [13]. Also, aimed at improving the spatial resolution of the NDT of metal pipes, a combination of transverse and longitudinal sensors was utilized to inspect different crack shapes of metal casings [15]. In [16], multi-pipe strings, which were required to protect oil and gas wells from by-products for safety considerations but made NDTs more difficult in terms of data interpretation, were inspected using the eddy-current diffusion properties of a TEM system with a multi-turn coil-based auxiliary sensor in the longitudinal direction. Similarly, the distortions of measured remote eddy-current field signal are analyzed and eliminated for pipeline inspection [17]. The above methods have been proven to be efficient for borehole TEM systems, as they improved the accuracy of downhole NDTs by reducing the influence of bad borehole conditions. However, in the field of borehole measurements, the sensors have to go through the wellbore to have an overall evaluation with respect to lots of periods that correspond to different borehole depths, where the nonconstant parameters of the temperature and motion speed lead to serious distortions that appear as baseline wanders (BWs) and motion-induced electromotive forces (EMFs) in the TEM response, thus strongly influencing the long-term precision.

So far, there are only minimal attempts that aimed to eliminate the influence of the nonconstant temperature and motion speed parameters on the downhole surveys. Generally, such influence is difficult and inefficient to suppress by repeatedly using measurement data from one or few periods, as both the temperature and motion speed would irregularly change with the increase of the borehole depth [8], [9]. Refer to [18], a temperature calibration procedure was employed to retrieve the temperature sensitivity of a fiber-optic distributed temperature sensing system that was used in downhole oil production. Also, [19] presented a temperature correction scheme that uses multiple temperature sensors to reduce temperature errors and help maintain accuracy over the entire temperature range. Following the same idea, a calibration module was developed to calibrate the temperature changes and parameter variations for a measurement system in a directional borehole radar [20]. The above methods are based on calibration coefficients to reduce the influence of the nonconstant parameters on borehole measurements. However, they are quite inefficient for borehole TEM systems, as too many measurement data that corresponds to a broad frequency range from early to late sampling times are involved in each signal period of the TEM signal because of the eddy-current diffusion properties in the time domain [3], [13]. Similar to the TEM denoising method in [21] and [22], [23] presented a discrete wavelet transform-based denoising method for borehole TEM data by employing a curve fitting technique. Furthermore, considering the effect of the motion measurement, a reference multi-turn receiver was used to cancel the magnetic background noise (MBN) effect in the main channel by employing the time domain property in each period [12]. However, the information from different periods were not exploited, and the influence of the temperature drifts was not corrected. By using multiple periods of TEM data in [24] and [25], the influence of BW and the noise caused by the motion measurement of the airborne TEM system were corrected with the wavelet transform and empirical mode decomposition (EMD) methods [26], [27], respectively. Although the EMD-based method was effective for the airborne TEM systems, the TEM response of different measurement periods were not separately processed, which made the denoising and BW correction performance for borehole TEM systems be strongly influenced by the magnetic hysteresis effect on the different sampling times.

In this paper, we present an EMD method based on borehole TEM array signal denoising and BW correction to compensate the variation in the temperature and motion measurement of downhole NDTs. Using the EMD algorithms, we analyzed the motion measurement and temperature drift effects on the performance of the borehole TEM system with respect to the MBN and effective permeability. Moreover, by formulating a three-dimensional borehole TEM data structure, we proposed an array-based ensemble EMD (AEEMD) method to improve the denoising performance of the borehole TEM signals. The effectiveness and accuracy of the proposed method were verified by applying it to an oil borehole TEM system to inspect an oil-well casing.

The rest of this paper is organized as follows. Based on the borehole TEM array signal model, the influence of the temperature drifts and MBN is presented in Section II. In Section III, we present the principle of the EMD approach for borehole TEM signal denoising and BW correction. An AEEMD method for improving the denoising performance of the borehole TEM signal is presented in Section IV and the experimental and simulation results are discussed in Section V. Finally, we conclude the paper in Section VI.

II. BOREHOLE TEM ARRAY SIGNAL MODEL

By considering a borehole TEM array system in a multi-cylindrically layered structure as shown in Fig. 1, with the electrical parameters (relative permeability, relative permittivity, and conductivity) and geometrical parameter of the jth layer being defined as μ_j, ε_j, σ_j, and r_j, respectively, we employed a single transmitter and M receivers with their number of turns given by N_{T} and N_{R}, respectively, where each receiver has the same number of turns.

As illustrated in Fig. 1, the transmitter continuously sends the TEM pulse, and the M receivers receive the TEM signals for each positive or negative period. Furthermore, with the movement of the borehole measurement system, each period

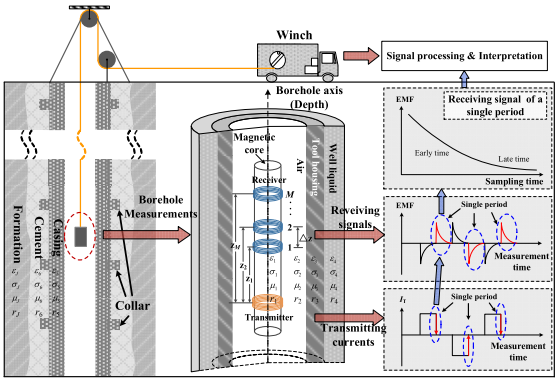

FIGURE 1. Borehole transient electromagnetic (TEM) array system.

corresponds to a borehole depth, where it is assumed that there is no displacement in a single measurement, and the measurement curves can be obtained by stacking the receiving signal of each period versus the borehole depth, where the negative period data have to be negated to maintain consistency. For each single period, the induced EMF of the mth receiver can then be calculated by [16]

$$U_m(z_m,\omega,\theta) = -i\omega\mu_1 N_R \int_0^{r_1} H_{z1}(z_m,\omega,\theta,r)\,2\pi r dr \quad (1)$$

where $H_{z1}(z_m,\omega,\theta,r)$ denotes the vertical component of the magnetic field for each single period with TRD z_m and radius r $(0 < r < r_1)$; θ is the thickness of the metal casings that can be expressed by r_5 - r_4 if only one casing is used [16], and z_m is the TRD between the mth receiver and the transmitting coil with an inter-element distance of Δz. The induced EMF in the time domain can then be obtained by the S-stage inverse Laplace transform method of Gaver–Stehfest with $i\omega = s\ln 2/t$ [13]:

$$U_m(z_m,t,\theta) = \frac{\ln 2}{t}\sum_{s=1}^{S} D_s U_m(z_m, s\ln 2/it,\theta) \quad (2)$$

where t and D_s denote the observation time and the integral coefficient of the Gaver–Stehfest inverse Laplace transform, respectively. According to the numerical approximation method of [13], (2) can be written into the vector form:

$$U_m(z_m,t,\theta) = \mathbf{x}(z_m)\cdot\mathbf{g}^{\mathrm{T}}(t,\theta) \quad (3)$$

where

$$\mathbf{g}(t,\theta) = \left[A_1 g_{1,1,1}(t,\theta),\ldots,A_Q g_{S,Q,P}(t,\theta)\right]_{1\times SQP} \quad (4)$$

$$\mathbf{x}(z_m) = \Bigg[\underbrace{\cos(\lambda_0 z_m\frac{B_1+1}{2}),\ldots,\cos(\lambda_0 z_m\frac{B_P+1}{2}),\ldots}_{P} \ldots,\underbrace{\cos(\lambda_0 z_m\frac{B_1+1}{2}),\ldots,\cos(\lambda_0 z_m\frac{B_P+1}{2})}_{P}\Bigg]_{1\times SQP} \quad (5)$$

denote the influence of the sampling time and geometric parameters of all the layers and the TRD, respectively. Also, λ_0 is a constant coefficient, P and Q represent the series of the two Legendre polynomials, and their quadrature coefficients and the zero-point are expressed by A and B, respectively. In the previous studies [13]–[16], to measure the thickness of the metal casings, the electrical and geometric parameters of all the layers except for the outer radius of the metal casing were assumed to be constant [16]. However, for a high-temperature borehole TEM system, not only the temperature drifts but also the magnetic hysteresis effect had a great influence, especially on the effective permeability μ_1 of the soft magnetic core [28]. On one hand, different borehole depths may correspond to different temperatures, which lead to irregularly changes of the effective permeability. On the other hand, since the TEM responses appear as typical exponential attenuation, the effective permeability of the TEM sensor at early and late times would be quite different due to the magnetic hysteresis effect, even though all the other system parameters are not changed. Thereby, to make a clear expression, we rewrote $\mathbf{g}(t,\theta)$ as $\mathbf{g}(t,\theta,T)$ to represent the influence of the electrical and geometric parameters with respect to the effective permeability μ_1, which is changed with both the sampling time t and the borehole temperature T. Moreover, we assumed that the induced EMFs of each receiver are discretely sampled with a sampling length L. Then, considering the effect of the MBN, the induced EMFs at the lth sampling time can be rewritten as

$$U_{m,l}(z_m,t_l,\theta,T) = \mathbf{x}(z_m)\cdot\mathbf{g}^{\mathrm{T}}(t_l,\theta,T) + n_{m,l}(t_l,T) \quad (6)$$

where $n_{m,l}(t_l,T)$ denotes the MBN that is caused by the motion-induced EMFs in the receiving coils due to the nonhomogeneous residue magnetic field of the metal casings. Moreover, the noise level increases with the increase of the sensors movement speed. In [25], the BW and the motion-induced EMFs for the airborne TEM systems could be corrected using the ensemble EMD (EEMD) method. However, the TEM responses of different measurement periods were not separately processed, which substantially led to a performance loss due to the magnetic hysteresis effect on the different sampling times. In this paper, we use θ_d and T_d to represent the casing thickness and temperature of the dth ($d = 1,\ldots,D$) depth. Then, the TEM response of the mth receiver and the lth sampling time for all depths can be obtained by staking (6) along the borehole axis, such that

$$\mathbf{U}_{m,l}(z_m,t_l,\boldsymbol{\theta},\mathbf{T}) = \left[U_{m,l}(z_m,t_l,\theta_1,T_1),\cdots,U_{m,l}(z_m,t_l,\theta_D,T_D)\right] \in \mathbb{C}^{1\times D} \quad (7)$$

where $\boldsymbol{\theta} = [\theta_1\ldots\theta_D]$ and $\mathbf{T} = [T_1\ldots T_D]$. By using the field experiments of an oil-well in the Shengli Oilfield of China as examples, the experimental sampling induced EMFs versus the borehole depths are demonstrated in Fig. 2 with a motion

speed of 300 m/h, where the TRD of the four receivers are 5 cm, 10 cm, 15 cm, and 20 cm, respectively.

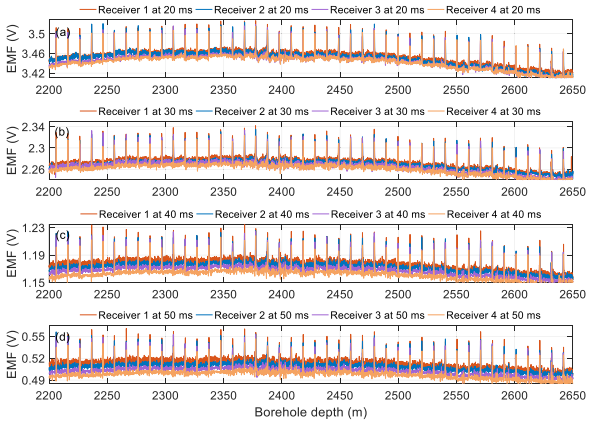

FIGURE 2. The experimental EMFs of the Receivers 1 to 4 versus the borehole depth with a speed of 300 m/h at (a) 20 ms, (b) 30 ms, (c) 40 ms, and (d) 50 ms.

From (7) and Fig. 2, it can be deduced that $M \times L$ EMF curves exist with respect to the different TRDs and the sampling times with the indices of m and l, respectively. Specifically, the recurring peaks denote the casing collars, and the TEM data was recorded according to the borehole depth. In the field of oil & gas production engineering, the wellbores are usually protected by metal casings, and the threaded collar is used to connect two joints of casing. Notably, the casing collars will substantially increase the thickness of the pipe strings and appear as many 'peaks' in the measured EMF curves. But fortunately, the positions of these collars are prior known for a certain oil-well, because the lengths of each casing are measured previously. Usually, by interpreting the induced EMF curves along with the borehole axis as thickness curves, the NDT of the downhole casings are realized. However, as shown in (7) and Fig. 2, the EMF curves are not only related to the sampling time and TRD, but they are also affected by the temperature drifts and the motion-induced EMFs, which appeared as BW and motion-induced noise, respectively, and which would have a great influence on the performance of the downhole NDTs.

III. THE EMD PRINCIPLE FOR THE BOREHOLE TEM SIGNAL

A. THE EMD OF THE BOREHOLE TEM SIGNAL

In Section II, we describe the effect of the temperature drifts and the motion-induced EMFs on the measurement curves of the borehole TEM array, which appear as the BW and undesired noise that influence the NDT performance in downhole casings. In addition, in this section, the use of the EMD approach for removing the BW and denoising the borehole TEM signals is demonstrated. According to the EMD principle in the matrix form, the borehole TEM response in (7) can be decomposed into K IMFs and a residue signal $\mathbf{R}(z_m, t_l, \boldsymbol{\theta}, \mathbf{T})$, such that [29]

$$\mathbf{U}_{m,l}(z_m, t_l, \boldsymbol{\theta}, \mathbf{T}) = \sum_{k=1}^{K} \mathbf{C}_k(z_m, t_l, \boldsymbol{\theta}, \mathbf{T}) + \mathbf{R}(z_m, t_l, \boldsymbol{\theta}, \mathbf{T}) \tag{8}$$

with

$$\mathbf{C}_k(z_m, t_l, \boldsymbol{\theta}, \mathbf{T}) = [C_k(z_m, t_l, \theta_1, T_1), \ldots, C_k(z_m, t_l, \theta_D, T_D)] \in \mathbb{C}^{1\times D} \tag{9}$$

$$\mathbf{R}(z_m, t_l, \boldsymbol{\theta}, \mathbf{T}) = [R(z_m, t_l, \theta_1, T_1), \ldots, R(z_m, t_l, \theta_D, T_D)] \in \mathbb{C}^{1\times D} \tag{10}$$

where the index k denotes the order of the IMFs. To simplify the expression, the residue signal can be defined to be the $K + 1$th IMF. By taking one of the experimental data in Fig. 2 from 2465 to 2545 m as an example, the TEM curve of the Receiver 2 at 30 ms can be decomposed into 9 IMFs, as shown in Fig. 3.

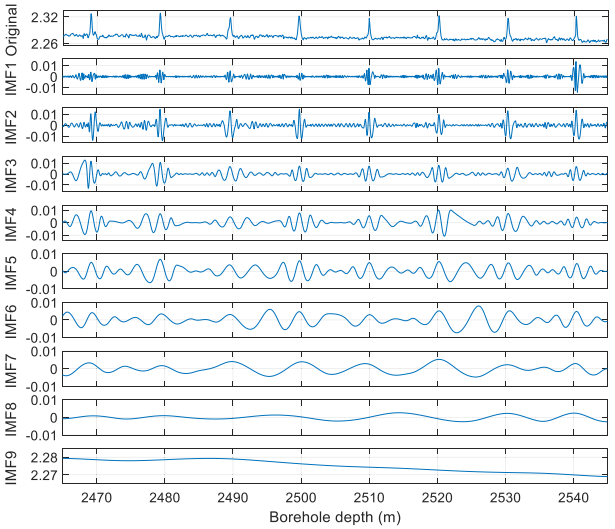

FIGURE 3. The EMD of the borehole TEM response of the Receiver 2 at 30 ms at a measurement speed of 300 m/h.

The first subfigure denotes the original data, and the 9 IMFs correspond to the different frequency components from high to low. Usually, it is assumed that the noise information is mainly included in the first several IMFs of the high-frequency components, while the baseline information is mainly included in the last several IMFs of the low-frequency components. In [29], the BW correction and the signal denoising can be realized by applying the windowing and filtering approach to the first and last several IMFs, respectively. According to the order determination method in [29], we define the first F orders as the noisy IMFs. As for the last E orders, they mainly correspond to the baseline components. For the BW correction, we apply a bank of low-pass filters to extract the BW components from the last E IMFs. Then, the residue part of the last E IMFs after

the BW correction can be written as:

$$\begin{aligned}&\mathbf{BWC}(z_m, t_l, \boldsymbol{\theta}, \mathbf{T})\\ &= \sum_{k=K-E+2}^{K+1} \mathbf{C}_k(z_m, t_l, \boldsymbol{\theta}, \mathbf{T})\\ &\quad - \sum_{k=K-E+2}^{K+1} \mathbf{LPF}^{\mathrm{T}}_{k-(K-E+1)} * \mathbf{C}_k(z_m, t_l, \boldsymbol{\theta}, \mathbf{T}) \quad (11)\end{aligned}$$

where $*$ is the convolution, and **LPF** denotes the low-pass filters. The cutoff frequencies of the low-pass filters are chosen according to [29]. In order to reduce the influence of the noise in the first F orders of the IMFs, the positions of the peaks of all the casing collars are utilized to form the denoising window. Then, for the noise reduction, we first apply a tapered cosine window $\boldsymbol{\psi}_k$ with two widths of τ_1 and τ_2 to all the collar peaks of the curve to reserve the collar information of the first F noise order of the EMD results. Then, we use a complementary window $\bar{\boldsymbol{\psi}}_k$ of the above window to suppress the noise information so that the residue signal of the first F IMFs after the noise suppression can be written as

$$\begin{aligned}\mathbf{DEN}(z_m, t_l, \boldsymbol{\theta}, \mathbf{T}) = \sum_{k=1}^{F} \big(&\mathbf{C}_k(z_m, t_l, \boldsymbol{\theta}, \mathbf{T}) \odot \boldsymbol{\psi}_k\\ &+ \alpha_k \cdot \mathbf{C}_k(z_m, t_l, \boldsymbol{\theta}, \mathbf{T}) \odot \bar{\boldsymbol{\psi}}_k\big) \quad (12)\end{aligned}$$

where $\odot$ denotes the inner product of the two vectors $0 < \alpha_k < 1$ is the attenuation coefficient and $\bar{\boldsymbol{\psi}}_k = \boldsymbol{\Gamma} - \boldsymbol{\psi}_k$, where $\boldsymbol{\Gamma} = [1, 1, \ldots, 1]_{1\times D}$. Clearly, the aim of the window function $\boldsymbol{\psi}_k$ is to retain the collar information. $\bar{\boldsymbol{\psi}}_k$ is used to suppress the collar information and retain the noise information. Its effect is contrary to that of $\boldsymbol{\psi}_k$. Here, $\bar{\boldsymbol{\psi}}_k$ is applied to the first F IMFs in conjunction with $\boldsymbol{\psi}_k$. Then, the BW correction and signal denoising results can be reconstructed by combining (11) and (12):

$$\begin{aligned}&\mathbf{U}'_{m,l}(z_m, t_l, \boldsymbol{\theta}, \mathbf{T})\\ &= \mathbf{DEN}(z_m, t_l, \boldsymbol{\theta}, \mathbf{T}) + \sum_{k=F+1}^{K-E+1} \mathbf{C}_k(z_m, t_l, \boldsymbol{\theta}, \mathbf{T})\\ &\quad + \mathbf{BWC}(z_m, t_l, \boldsymbol{\theta}, \mathbf{T}) \quad (13)\end{aligned}$$

In (13), the second term represents the middle IMFs that neither contain noise components nor baseline components.

B. EFFECT OF THE MEASUREMENT SPEED ON THE EMD

The EMD-based signal denoising and BW correction in Section III.A are effective for the experiment curves shown in Fig. 2 at a measurement speed of 300 m/h. However, in the case of the borehole measurement, the motion speed of the sensor would have a great influence on the performance of the EMD for the TEM signals, as a fast motion speed may not only make the noise strong, but it can also reduce the effective number of measurement points in a certain range of borehole depths.

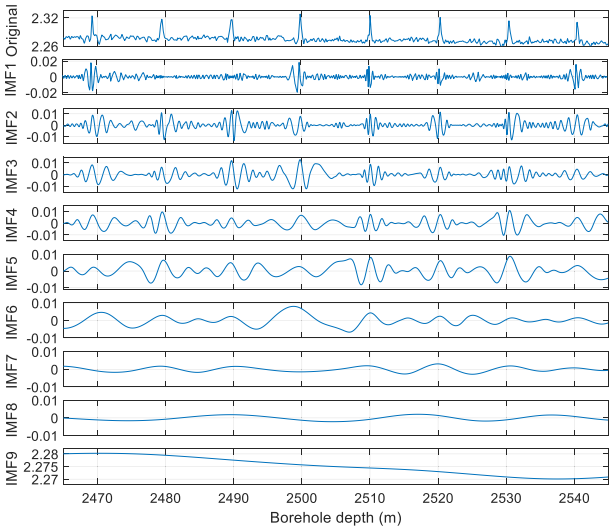

FIGURE 4. The EMD of the borehole TEM response of the Receiver 2 at 30 ms at a measurement speed of 600 m/h.

In Fig. 4, we show the original data and the EMD results at a measurement speed of 600 m/h, to be compared with Fig. 3, where the experimental data are also chosen from the 2465 to 2545 m range of the Receiver 2 at 30 ms. Obviously, the original data with the different measurement speeds have the same collar locations and the same mean value of the induced EMFs, but the noise strength and the number of effective measurement points are different. Furthermore, by comparing the EMD results of Fig. 3 and 4 with measurement speeds of 300 m/h and 600 m/h, respectively, it can be seen that the difference of the lower-order IMFs between the two different measurement speeds is much larger than that of the higher-order IMFs. Especially, in comparison with Fig. 3, there is a more serious EMD aliasing in the first F IMFs in Fig. 4, where the peaks with respect to the casing collar are mixed with the noise component. To further investigate this problem, the BW and noise components of the EMD results of the different measurement speeds are compared. For convenience, the sum of the first F IMFs is used to represent the most part of the noise component and express the noise level because noise is mainly included in the first F IMFs. Then, the correspondence of the noise component in the sum of the first F IMFs $\mathbf{U}_{\mathrm{N}}(z_m, t_l, \theta, \mathbf{T})$ and the estimated baseline components $\mathbf{U}_{\mathrm{BW}}(z_m, t_l, \theta, \mathbf{T})$ can be represented as

$$\mathbf{U}_{\mathrm{N}}(z_m, t_l, \boldsymbol{\theta}, \mathbf{T}) = \sum_{k=1}^{F} \mathbf{C}_k(z_m, t_l, \boldsymbol{\theta}, \mathbf{T}) \quad (14)$$

$$\mathbf{U}_{\mathrm{BW}}(z_m, t_l, \boldsymbol{\theta}, \mathbf{T}) = \sum_{k=K-E+2}^{K+1} \mathbf{LPF}^{\mathrm{T}}_{k-(K-E+1)} * \mathbf{C}_k(z_m, t_l, \boldsymbol{\theta}, \mathbf{T}) \quad (15)$$

By using the above equations to process the EMD results in Fig. 3 and 4, the two EMF curves of the borehole TEM data and their noise and baseline correspondence in Fig. 5

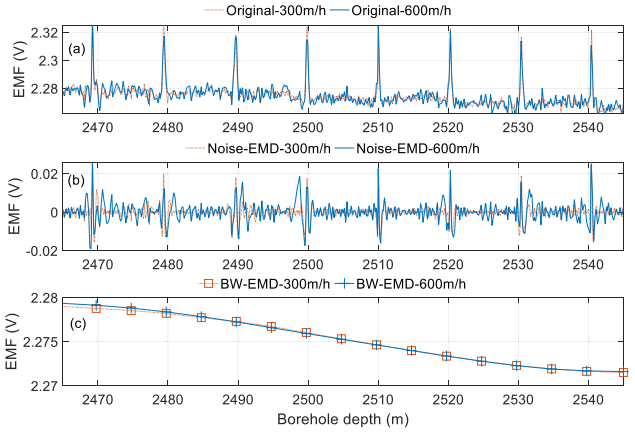

FIGURE 5. Comparison of (a) the two EMF curves of the experimental data, (b) their noise, and (c) baseline wander correspondence with measurement speeds of 300 m/h and 600 m/h, respectively.

($E = 2, F = 3$) are compared based on the same parameters except for the measurement speeds of 300 m/h and 600 m/h, respectively.

It can be observed from Fig. 5 that the noise components of the different motion speeds are quite different, while the BW components are almost the same. Specifically, the noise strength of the case with the speed of 600 m/h becomes much larger than that with the speed of 300 m/h. Also, the noise component near the position of each casing collar is particularly strong and seems to be caused by the non-suitable cutting-off of the window function, which is actually due to the mode aliasing of the casing collars peak and the noise peaks. On one hand, the effect of the high temperature range, which appeared as various BWs, does not change with the motion speed, and can easily be removed using the BW correction principle of Section III.A. On the other hand, the MBN effect, which appeared as motion-induced EMFs, is closely related to the motion speed, since faster speeds may not only correspond to stronger MBN values but also to more serious mode aliasing due to the reduction of the number of effective points in a certain measurement depth range. Although the stronger noise can be suppressed by modifying the attenuation coefficients in (12), the distortion of the noise component, which becomes stronger near the position of each casing collar, cannot be easily cancelled.

IV. AEEMD FOR BOREHOLE TEM SIGNAL DENOISING

A. THE EEMD FOR THE BOREHOLE TEM SIGNAL

In Section III, we showed the principle of the EMD approach for the borehole TEM signal denoising and BW correction. However, since the noise component is closely related to the motion speed of the sensors, the noise suppression performance of the borehole TEM signal with the fast measurement speed would be significantly decreased. Thus, to improve the signal denoising effect, the EEMD algorithm [25], a noise-assisted data analysis, was developed to eliminate the mode aliasing of the IMFs. According to the EEMD method, the jth stage of the noise-aided data of (7) can be formulated by

$$\mathbf{U}_{m,l,j}(z_m, t_l, \boldsymbol{\theta}, \mathbf{T}) = \mathbf{U}_{m,l}(z_m, t_l, \boldsymbol{\theta}, \mathbf{T}) + \mathbf{n}'_j(z_m, t_l, \boldsymbol{\theta}, \mathbf{T}) \tag{16}$$

where $\mathbf{n}_j'(z_m, t_l, \theta, \mathbf{T})$ denotes the jth artificial identically independently distributed (I.I.D.) Gaussian white noise. In this paper, we chose to add noise of an amplitude that is about 0.2 standard deviation of that of the data. By using the EMD-based borehole TEM system model in Section III, the EEMD can be expressed by averaging the EMDs of the J noise-aided data as follows

$$\hat{\mathbf{U}}_{m,l}(z_m, t_l, \boldsymbol{\theta}, \mathbf{T}) = \sum_{k=1}^{K} \mathbf{C}_{k\text{-EEMD}}(z_m, t_l, \boldsymbol{\theta}, \mathbf{T}) + \mathbf{R}_{\text{EEMD}}(z_m, t_l, \boldsymbol{\theta}, \mathbf{T}) \tag{17}$$

where

$$\mathbf{C}_{k\text{-EEMD}}(z_m, t_l, \boldsymbol{\theta}, \mathbf{T}) = \frac{1}{J}\sum_{j=1}^{J} \mathbf{C}_{j,k}(z_m, t_l, \boldsymbol{\theta}, \mathbf{T}) \tag{18}$$

$$\mathbf{R}_{\text{EEMD}}(z_m, t_l, \boldsymbol{\theta}, \mathbf{T}) = \frac{1}{J}\sum_{j=1}^{J} \mathbf{R}_j(z_m, t_l, \boldsymbol{\theta}, \mathbf{T}) \tag{19}$$

denote the kth IMF and residue term of the EEMD, respectively. $\mathbf{C}_{j,k}(z_m, t_l, \theta, \mathbf{T})$ and $\mathbf{R}_j(z_m, t_l, \theta, \mathbf{T})$ denote the kth IMF and the residue signal of the jth noise-aided data, respectively. As we all know, the EEMD method belongs to a class of noise-assisted EMD methods that are aimed at alleviating mode mixing caused by noise and signal intermittency. The use of the EEMD will substantially improve the signal denoising performance for the borehole detection in this paper. Usually, we need to estimate the noise variation for the generation of artificial noise with Gaussian distribution. However, in the field of borehole detection, the noise variance would irregularly change due to the bad borehole conditions that come with the increase of the borehole depth with respect to change of temperatures and pressures. So under this situation, the generation of the artificial noise data for the EEMD method will become difficult and time consuming for in-time NDTs. In order to solve this problem, we herein present an AEEMD denoising method for the borehole TEM system.

B. THE THREE-DIMENSIONAL STRUCTURE OF THE BOREHOLE TEM ARRAY DATA

By stacking the induced EMF of each receiver in (6), the matrix form of the received signal of the uniform linear multi-coil array on the dth depth can be expressed, such that

$$\mathbf{U}_{1-M,1-L,d} = \begin{bmatrix} \mathbf{x}(z_1)\cdot\mathbf{g}^{\mathrm{T}}(t_1,\theta_d,T_d) & \cdots & \mathbf{x}(z_1)\cdot\mathbf{g}^{\mathrm{T}}(t_L,\theta_d,T_d) \\ \mathbf{x}(z_2)\cdot\mathbf{g}^{\mathrm{T}}(t_1,\theta_d,T_d) & \cdots & \mathbf{x}(z_2)\cdot\mathbf{g}^{\mathrm{T}}(t_L,\theta_d,T_d) \\ \vdots & \ddots & \vdots \\ \mathbf{x}(z_M)\cdot\mathbf{g}^{\mathrm{T}}(t_1,\theta_d,T_d) & \cdots & \mathbf{x}(z_M)\cdot\mathbf{g}^{\mathrm{T}}(t_L,\theta_d,T_d) \end{bmatrix}$$

$$+\begin{bmatrix} n_{1,1}(t_1,T_d) & n_{1,2}(t_2,T_d) & \cdots & n_{1,L}(t_L,T_d) \\ n_{2,1}(t_1,T_d) & n_{2,2}(t_2,T_d) & \cdots & n_{2,L}(t_L,T_d) \\ \vdots & \vdots & \ddots & \vdots \\ n_{M,1}(t_1,T_d) & n_{M,2}(t_2,T_d) & \cdots & n_{M,L}(t_L,T_d) \end{bmatrix}_{M\times L} \tag{20}$$

In (20), each element of the noise matrix can be assumed to be I.I.D., as the measurement conditions of each receiver at different sampling times are almost the same. Similar to (7), the response of the TEM array for all depths can be obtained by staking (20) along with the borehole axis, such that

$$\mathbf{U}_{1-M,1-L,1-D} = \left\{\mathbf{U}_{1-M,1-L,1} \;\; \mathbf{U}_{1-M,1-L,2} \;\; \cdots \;\; \mathbf{U}_{1-M,1-L,D}\right\}_{M\times L\times D} \tag{21}$$

It can be observed from (21) that the borehole TEM array data correspond to a three-dimensional structure, where the three axes are represented by the M receivers, L sampling times, and D depths (also known as D measurement times). In order to distinguish the two 'time', we define the sampling time and measurement time as the fast time and slow time, respectively. Considering the motion speed, each measurement period in the slow time would correspond to a borehole depth, as shown in Section II (depth = speed × measurement time), and would also comprise the sampling data of the fast time from the early time t_1 to the late-time t_L with respect to receivers 1 to M. Specifically, the 3-D data structure of the borehole TEM array is shown in Fig. 6.

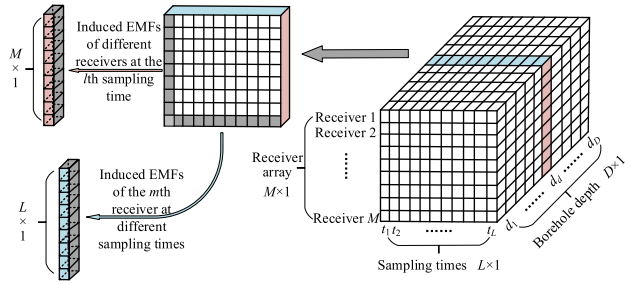

FIGURE 6. The 3-D data structure of the borehole TEM array.

From Fig. 6, it can be observed that $M \times L$ independent TEM data curves exist along with the borehole axis with the D depths, where each of them has a model, as shown in Section II, and can be processed using the EMD principles. If the common information of the $M \times L$ data can be used to realize the EEMD, the artificial noise-aided procedure can be substantially reduced. Here, the EMD and EEMD are applied on univariate signals (a function of depth). Although the borehole TEM array data can be expressed as 3-D structure, where the induced EMFs are with respect to the depth (D), the sampling times (L), and the receivers (M), the effect of the three variables are quite different. Firstly, the BW and noise of the borehole TEM data are mainly caused by the change of the depth as illustrated in Section II. Secondly, the dimension of the M (*e.g.* 8) and L (*e.g. 50*) are not long enough to realize the EMD and EEMD algorithms. Thirdly, only when we treat the TEM data as a function of depth channel-by-channel with each of them corresponding to a specified m and l, just as shown in Fig. 2, the TEM data appear as the $M \times L$ EMF curves with the same positions of recurring peaks of the casing collar, thus offering an opportunity to process all of these EMF curves using the EMD and EEMD with the same denoising window. In order to analyze the common information of the $M \times L$ data curves, we here compare the normalized induced EMFs of 7 cases, as shown in Fig. 7, including Receiver 1 at 20 ms, Receiver 1 at 30 ms, Receiver 1 at 40 ms, Receiver 1 at 50 ms, Receiver 2 at 30 ms, Receiver 3 at 30 ms, and Receiver 4 at 30 ms, where the experimental parameters are the same as in Fig. 4 at a measurement speed of 600 m/h.

For the L-dimension of Fig. 7, it can be observed that the TEM data of the same receiver at different sampling times are similar because of the eddy-current diffusion property of the TEM system, indicating the great similarity between these cases after the cancellation of the BW information. However, for the M-dimension, the difference in the TEM data of the different receivers is mainly manifested as 'phase' shifting [13] along with the longitudinal (borehole) axis due to the difference in the TRDs.

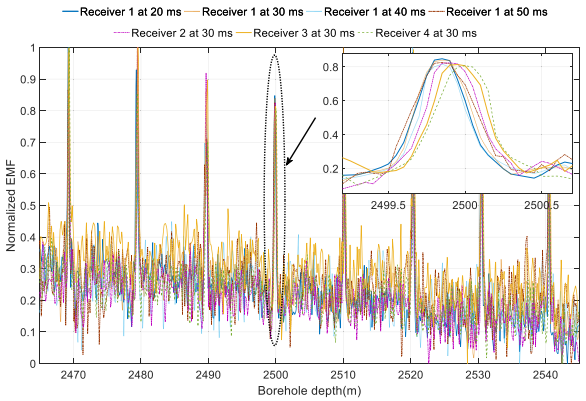

FIGURE 7. Comparison of the normalized EMFs of different data curves.

C. THE AEEMD METHOD

Different to the original EEMD method that uses lots of artificial noise data, the AEEMD method proposed in this paper involves a dimension reduction operation by employing the M and L data with their common information and I.I.D. noise to improve the denoising performance. The procedure of the AEEMD method is shown in Algo. 1.

The procedure of the AEEMD method contains four basial steps for the BW correction and signal denoising, the array weighting, EMD decomposition, BW correction, and the L-stage EEMD. The details of the implementation of the proposed AEEMD method are shown as follows.

Firstly, in order to make use of the M-dimension data, we apply an array weighting approach to the lth column of (20) to compensate for the 'phase' shifting by cancelling

Algorithm 1 AEEMD

Require: $\mathbf{U}_{m,l}(z_m, t_l, \theta, \mathbf{T})$, $m = 1, 2, \ldots, M$; $l = 1, 2, \ldots, L$;

1: Apply an array weighting approach to M EMF curves (M-dimension data) with the same sampling times l ($l = 1, 2, \ldots, L$);
2: Decompose the array output into $K + 1$ IMFs for all l ($l = 1, 2, \ldots, L$) using the EMD principle;
3: Apply a bank of low-pass filters to extract the BW components of the L EMD results to achieve the BW correction;
4: Use the EEMD method to the L EMD results (L-dimension data) after BW correction to further denoise with dimension reduction.

the effect of the TRDs, according to [13]:

$$y_{l,d} = \mathbf{W}^{\mathrm{T}}\mathbf{U}_{1-M,l,d} = \sum_{m=1}^{M} w_m U_{m,l}(z_m, t_l, \theta_d, T_d) \quad (22)$$

where $\mathbf{W} = [w_1 w_2 \ldots w_M]^{\mathrm{T}}$. The shifting can be compensated by weighting the array output to be subjected to the response of the receiver with $z = 0$ using the linearly constrained minimum variance criterion. Moreover, considering the I.I.D. noise of the array receiving, we can use the EMD of the array weighting output to improve the SNR, which is also an averaged dimension reduction operation like the M-stage EEMD. Note that although the shifting may be removed by other methods besides the array weighting, all methods are mainly averaging operations as well as the dimension reduction of the M receivers.

Secondly, by applying an EMD to the array outputs, we can obtain L EMD results, where each of them contains $K + 1$ IMFs. The EMD of the weighted borehole TEM array can be calculated by substituting (8) and (22) into (21):

$$\begin{aligned}\mathbf{Y}_l &= \begin{bmatrix} y_{l,1} & y_{l,2} & \cdots & y_{l,D} \end{bmatrix}_{1\times D} \\ &= \sum_{k=1}^{K} \mathbf{C}_{Y,k}(t_l, \boldsymbol{\theta}, \mathbf{T}) + \mathbf{R}_Y(t_l, \boldsymbol{\theta}, \mathbf{T}) \end{aligned} \quad (23)$$

where $\mathbf{C}_{Y,k}(t_l, \theta, \mathbf{T})$ and $\mathbf{R}_Y(t_l, \theta, \mathbf{T})$ denote the kth IMF and residual signal ($K + 1$th IMF) of the EMD results of $\mathbf{Y}_l$, respectively.

Thirdly, by cancelling the BW component again with the EMD principle for the borehole TEM signals in Section III, the residue part of the weighted array signal can be expressed as

$$\mathbf{Y}_{l-\mathrm{Residue}} = \mathbf{Y}_l - \mathbf{Y}_{l-\mathrm{BW}} \quad (24)$$

where

$$\mathbf{Y}_{l-\mathrm{BW}} = \sum_{k=K-E+2}^{K+1} \mathbf{LPF}^{\mathrm{T}}_{k-(K-E+1)} * \mathbf{C}_{Y,k}(t_l, \boldsymbol{\theta}, \mathbf{T}) \quad (25)$$

represents the BW component of $\mathbf{Y}_l$ according to (15). Following the EEMD idea and considering the similarity between the TEM data at different sampling times after the cancellation of the BW information, we can directly average the data of different sampling times in (24) to further reduce the dimension.

Finally, using the EEMD method that averages of the obtained modes by the EMD of the L dimension data, and can be further denoised with EMD principle for the borehole TEM signals in Section III. Then, the AEEMD can be expressed as

$$\begin{aligned}\mathbf{Y}_{\mathrm{AEEMD}} &= \frac{1}{L}\sum_{l=1}^{L} \mathbf{Y}_{l-\mathrm{Residue}} \\ &= \sum_{k=1}^{K} \mathbf{C}_{k-\mathrm{AEEMD}}(\boldsymbol{\theta}, \mathbf{T}) + \mathbf{R}_{\mathrm{AEEMD}}(\boldsymbol{\theta}, \mathbf{T}) \end{aligned} \quad (26)$$

where

$$\begin{aligned}&\mathbf{C}_{k-\mathrm{AEEMD}}(\boldsymbol{\theta}, \mathbf{T}) \\ &= \begin{cases} \dfrac{1}{L}\displaystyle\sum_{l=1}^{L} \mathbf{C}_{Y,k}(t_l, \boldsymbol{\theta}, \mathbf{T}) & 1 \le k < K - E + 2 \\ \dfrac{1}{L}\displaystyle\sum_{l=1}^{L} \left(\mathbf{C}_{Y,k}(t_l, \boldsymbol{\theta}, \mathbf{T}) - \mathbf{LPF}^{\mathrm{T}}_{k-(K-E+1)} * \mathbf{C}_{Y,k}(t_l, \boldsymbol{\theta}, \mathbf{T})\right) & \\ \qquad\qquad K - E + 2 \le k \le K \end{cases} \end{aligned} \quad (27)$$

and $\mathbf{R}_{\mathrm{AEEMD}}(\theta, \mathbf{T})$ has the same expression as $\mathbf{C}_{k-AEEMD}(\theta, \mathbf{T})$ with $k = K+1$. As illustrated in (20), the noise of the L-dimension data are still I.I.D., thus allowing the averaging of the L-dimension data to form an L-stage EEMD. By using the AEEMD method, no artificial noise is needed, which substantially improve the efficiency of the denoising procedure. Moreover, the use of the array weighting can achieve a pre-improvement of the SNR, the denoising performance can be also improved as long as the sizes of M and L are great enough. It has to be mentioned that since this approach makes an assumption that the signals of the different sampling times are almost the same after the cancellation of the BW information, as shown in Fig. 7, the sampling time should be as late as possible to ensure the similarity of the array data. Thereby, the main shortcoming of the proposed AEEMD method is that it is not suitable for the early time TEM data denoising.

V. FIELD EXPERIMENTS

A. EXPERIMENTAL RESULTS

The validity of the AEEMD method for borehole TEM array signal denoising and BW correction was confirmed by field experiments for the NDT of downhole casings. The experiments were conducted in a production oil well of the Dongxin oil production plant in Shengli Oilfield, China, with standardized $5^{1/2}$-inch metal casings, and the parameters of the borehole TEM array system are shown in Table 1.

In our experiment, we chose the EMF curve of Receiver 2 at 30 ms from 2465 to 2545 m with measurement speed

TABLE 1. Parameters of the borehole TEM array system units for magnetic properties.

Parameter	Symbol	Value
Radius of the multi-coil array sensor	r_1	12 mm
Number of receivers	M	8
Inter-element spacing	Δz	50 mm
Tool housing inner radius	r_2	18.5 mm
Tool housing outer radius	r_3	21.5 mm
Standardized casing inner radius	r_4	62.13 mm
Standardized casing outer radius	r_5	69.85 mm
Cement ring outer radius	r_6	88.9 mm

of 600 m/h as the EMD and EEMD data, and all $M \times L$ EMF curves were employed in the AEEMD, where all the data were repeatedly experimented with different measurement speeds, and the corresponding temperature range was approximately from 99 to 104 °. The experimental conditions, including the measurement speeds, the temperature range, the casing thickness, and the casing structures, are shown in Fig. 8.

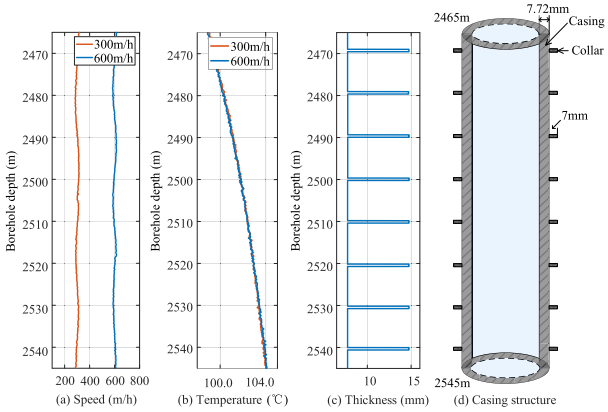

FIGURE 8. Experimental conditions from 2465 to 2545 m, including (a) the measurement speeds, (b) temperature range, (c) casing thickness, and (d) casing structure.

In Fig. 8, two typical measurement speeds of 300 m/h and 600 m/h were approximately implemented, where the temperatures curves at different speeds were almost the same. The metal pipe string has a thickness of 7.72 mm and an outer diameter of 139.7 mm, where each casing is connected by a collar with a thickness of approximately 7 mm. Thus, the corresponding thickness in the collar becomes 14.72 mm [16]. Notably, the metal casings thickness can sometimes suffer from various damages resulting from corrosive well liquids, scrapes of various downhole tools, which non-homogeneously decreases their thickness. In that case, the NDT of the residue thickness has to be implemented to evaluate the safety of the oil-well casing.

Fig. 9 and 10 show the comparison of the proposed AEEMD and original EEMD results of the borehole TEM system, where the ensemble stages of the noise-aided data of the Fig. 9 and 10 were set to 80 ($M = 4$ and $L = 20$ for AEEMD) and 400 ($M = 8$ and $L = 50$ for AEEMD), respectively. We can observe from Fig. 9 and 10 that, on the

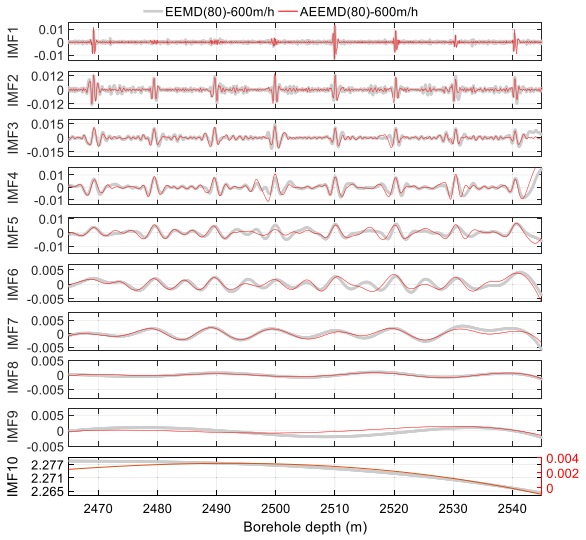

FIGURE 9. Comparison of the proposed AEEMD and original EEMD results of the borehole TEM array data with the ensemble stages of the noise-aided data of 80 (M=4 and L=20 for AEEMD) at a measurement speed of 600 m/h.

basis of the ensemble average operation, the mode mixing can be cancelled effectively for both the AEEMD and EEMD methods. However, as illustrated in Section IV, the EEMD method performed better than the original EMD method with a large number of stages of the noise-aided data, which is required for suppressing the influence of the mode aliasing due to the fast motion measurement, thus making the borehole system inefficient for implementation. As an alternative, the AEEMD method made use of the array data from the two dimensions of the M receivers and the L late sampling times. Furthermore, by comparing Fig. 9 and 10, the difference in the AEEMD and EEMD results is mainly manifested in the first two and last IMFs. As shown in Fig. 9 and 10, the noise level in the first two IMFs of the proposed AEEMD method is lower than that of the EEMD method, especially for the small number of stages. This is because that the array weighting approach of AEEMD method can achieve a pre-improvement of the SNR. In addition, when the number of stages is not great enough, the artificial noise introduced in the EEMD method cannot be cancelled effectively. Moreover, since the L-stage ensemble operation of the AEEMD does not introduce any artificial noise, but the I.I.D. noise of different sampling times, the total noise level will be lower even small number of stages can be used. In the last IMF (IMF 10), which includes the BW components, the EEMD results are almost the same as those of the IMF 9 of EMD results in Fig. 3 and 4 since the BW is not affected by the motion speed. In contrast, there are no BWs in the IMF 10 of the AEEMD because the BW component was removed in advance with the AEEMD method, as shown in Section IV.C.

B. ANALYSES AND DISCUSSION

In order to demonstrate the effectiveness of the proposed method, in Fig. 11, we compared the noise correspondence (the sum of the first three IMFs) of the AEEMD and EEMD

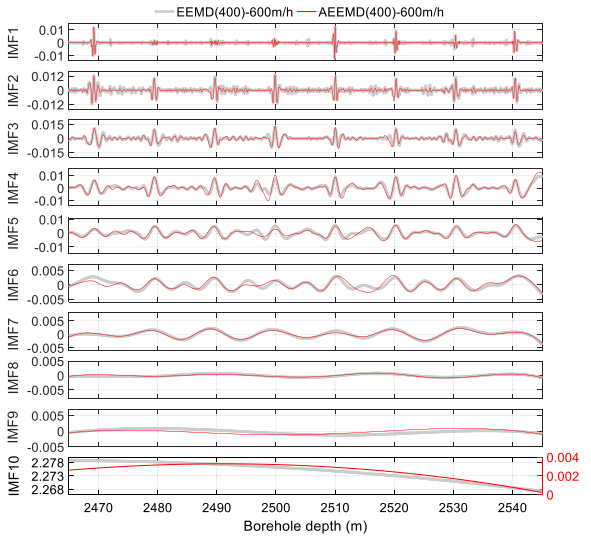

FIGURE 10. Comparison of the proposed AEEMD and original EEMD results of the borehole TEM array data with the ensemble stages of the noise-aided data of 400 (M=8 and L=50 for AEEMD) at a measurement speed of 600 m/h.

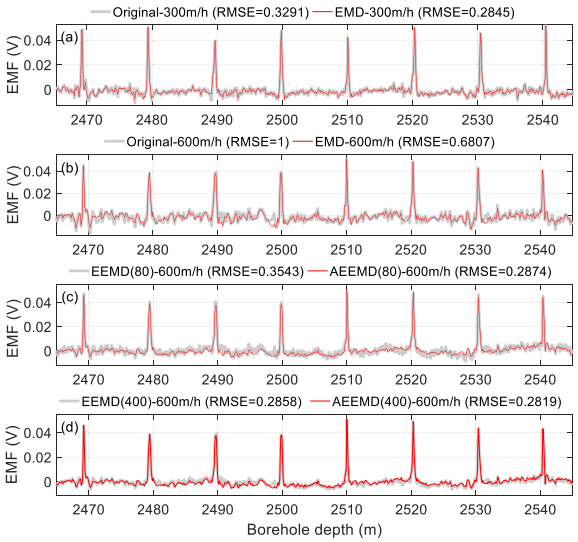

FIGURE 12. Comparison of the BW correction and denoising results of different cases, including (a) Original-300 m/h and EMD-300 m/h, (b) Original-600 m/h and EMD-600 m/h, (c) EEMD (80)-600 m/h and AEEMD (80)-600 m/h, and (d) EEMD (400)-600 m/h and AEEMD (400)-600 m/h.

methods at a measurement speed of 600 m/h, with ensemble number of 80 and 400, respectively.

It can be observed from Fig. 11 that the noise level of both the EEMD-600 m/h and AEEMD-600 m/h are much lower than that of the EMD-600 m/h as shown in Fig. 5. As a comparison, the EEMD method with the small ensemble number of 80 performs not well because the artificial noise is not cancelled effectively, but the AEEMD with 80 stages can almost reach the level of the EEMD method with 400 stages. Moreover, in the case of ensemble number is great enough of 400, the AEEMD also has relative lower noise level since the array weighting can achieve an improvement of SNR previously.

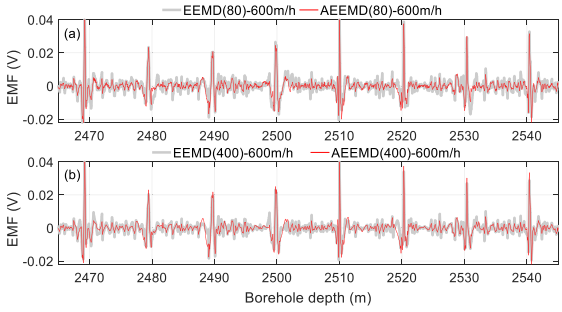

FIGURE 11. Comparison of the noise correspondence of EEMD-600 m/h and AEEMD-600 m/h with (a) 80 stages; (b) 400 stages.

In order to further analyze the performance of the proposed AEEMD method, we compared the BW correction and denoising results of the above cases and the original measurement curves at a motion speed of 300 m/h and 600 m/h, as shown in Fig. 12, where the BW components were removed to make the comparison more clearly. In our experiments, we define an ideal case that was taken by an almost static measurement with a maximum motion speed that did not exceed 30 m/h, whose original measurement curves are not influenced by the motion measurements, and where the noise level may be sufficiently reduced by averaging the repeated measurement points along with the borehole axis. On this basis, we also removed the BW correspondence of the static measurement to represent the ideal case. Without a loss in generality, we employed the normalized root-mean-square error (RMSE) of different cases in comparison with the ideal case in Fig. 12, where the RMSE is defined as:

$$\mathrm{RMSE} = \sqrt{\frac{1}{D}\sum_{d=1}^{D}\left(\Delta\left(d\right) - \mathrm{Ideal}\left(d\right)\right)^2} \tag{28}$$

where $\Delta(d)$ denotes the different cases of the data curves, including the data after the BW correction and the denoising process using the EMD, EEMD, and AEEMD. From Fig. 12, it can be observed that the lower the motion speed, the better the denoising performance. However, a low motion speed also signifies a low efficiency, which would be inefficient for borehole measurement systems. Thereby, an appropriate motion speed is always required to maintain both the measurement performance and efficiency. As shown in Fig. 12(b), when the speed is increased to 600 m/h, the noise level obviously increases, and the EEMD and the proposed AEEMD method could significantly improve the denoising performance of the borehole TEM system for NDTs in downhole casings, as shown in Fig. 12(c) and (d). Also, with only 80 stages, the AEEMD method could achieve similar performance in comparison with the EEMD method with 400 stages. To make a clear description of the AEEMD method on the denoising performance for the borehole TEM array, we set $M = 1, 2, 4,$ and 8 and $L = 1 \ldots 50$, so that the number of stages of the noised-aided data of the AEEMD method is changed

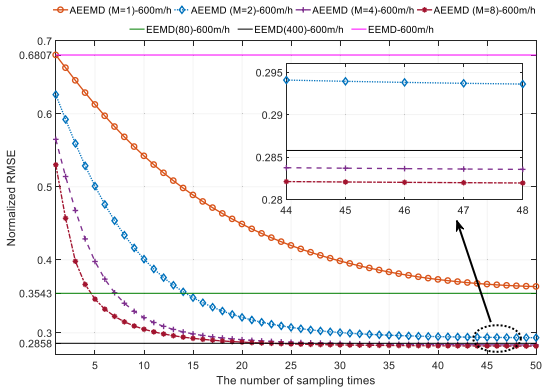

FIGURE 13. Normalized root-mean-square error (RMSE) of the different cases of the data curves.

from 1 to 400. Since the ideal case is used as the standard one in RMSE, it appears as the straight line with all the RMSEs=0. Moreover, all the RMSEs of the different cases are normalized by the maximum RMSE that corresponds to the worst case of the original data at a measurement speed of 600 m/h, which appears as the curve of RMSEs=1. The experimental results are shown in Fig. 13.

Obviously, the AEEMD and EEMD methods could significantly improve the denoising performance. By increasing $M \times L$, which denotes the number of stages of the noise-aided data for the AEEMD, the RMSE correspondingly decreased, where both the M-dimension of the number of receivers and the L-dimensions of the number of the late sampling times could improve the denoising performance. Specifically, when $M \times L$ was great enough, the RMSE level of AEEMD became a little lower than the EEMD method, which is due to the improved SNR of the array weighing and data averaging without introducing extra noise. Moreover, we can also find that when L was great enough with $L = 50$, the case with $M = 1$ still had a great performance loss due to the small number of $M \times L$. Notably, simply increasing M or L separately cannot achieve ideal performance, as a too large number of M and L may lead to a certain degree of distortion due to the decreased signal strength of the large TRDs and because of the too-long sampling time. Therefore, reasonable values of M and L can not only increase the denoising performance but can also improve the efficiency of the borehole TEM system. Thus, optimizing the M and L values for borehole TEM array signal denoising needs to be further investigated in future studies. It has to be mentioned that since the proposed procedures are all based on the principle of original EMD and EEMD methods, we made comparisons only between the proposed AEEMD method and the original EMD as well as EEMD methods. If we replace the original EMD and EEMD method by using some advanced EMD-based methods, such as the median EEMD [30] and multivariate EMD [31], the corresponding performance improvement gained from the advanced EEMD method can be also inherited; and this would be an interesting research direction to further improve the denoising performance to the borehole TEM system.

VI. CONCLUSION

In this study, EMD-based borehole TEM array signal denoising and BW correction methods were proposed to compensate for the bad measurement conditions in downhole NDTs. Considering the motion measurement and effective permeability, we investigated the effects of the MBN and temperature drift, and it was shown that the BW could be effectively removed with the EMD approach, but the signal denoising performance was significantly affected by the measurement speed of the downhole NDT sensors. Moreover, we proposed an AEEMD method to improve the denoising performance of the borehole TEM signals, and the generation of the noise-aided data could be improved by employing the borehole TEM array. The conducted experiments in a standardized oil-well casing demonstrated the effectiveness of the proposed system.

ACKNOWLEDGMENT

The authors would like to thank the reviewers for their helpful suggestions, which have considerably improved the quality of the manuscript.

REFERENCES

[1] F. Liu, J. Lin, Y. Wang, S. Wang, X. Cao, and B. Chen, "Design of cable parallel air-core coil sensor to reduce motion-induced noise in helicopter transient electromagnetic system," *IEEE Trans. Instrum. Meas.*, vol. 68, no. 2, pp. 525–532, Feb. 2019.

[2] J. E. Danielsen, E. Auken, F. Jørgensen, V. Søndergaard, and K. I. Sørensen, "The application of the transient electromagnetic method in hydrogeophysical surveys," *J. Appl. Geophys.*, vol. 53, no. 4, pp. 181–198, Oct. 2003.

[3] L. Zhao, C.-J. Li, Z.-X. Duan, W. Wang, and X.-D. Wu, "The metal thickness detection using pulsed eddy-current computation and detection method," *Cluster Comput.*, vol. 22, no. S3, pp. 6551–6562, May 2019.

[4] X. Chen and J. Li, "Pulsed eddy current testing for electromagnetic parameters of a spherical conductor," *IEEE Sensors J.*, vol. 20, no. 7, pp. 3627–3635, Apr. 2020.

[5] H. Yang, S. Chen, J. Yue, F. Li, and H. Zhang, "Transient electromagnetic response with a ramp current excitation using conical source," *IEEE Access*, vol. 7, no. 5, pp. 63829–63836, May 2019.

[6] G. Piao, J. Guo, T. Hu, Y. Deng, and H. Leung, "A novel pulsed eddy current method for high-speed pipeline inline inspection," *Sens. Actuators A, Phys.*, vol. 295, pp. 244–258, Aug. 2019.

[7] D. I. Ona, G. Y. Tian, R. Sutthaweekul, and S. M. Naqvi, "Design and optimisation of mutual inductance based pulsed eddy current probe," *Measurement*, vol. 144, pp. 402–409, May 2019.

[8] B. R. Spies, "Electrical and electromagnetic borehole measurements: A review," *Surv. Geophys.*, vol. 17, no. 4, pp. 517–556, Jul. 1996.

[9] A. I. Mohammed, B. F. Oyeneyin, B. Atchisonb, and J. Njuguna, "Casing structural integrity and failure modes in a range of well types—A review," *J. Natural Gas Sci. Eng.*, vol. 68, pp. 1–9, Jun. 2019.

[10] Y. A. Plotnikov, F. W. Wheeler, S. Mandal, W. R. Ross, J. S. Price, E. J. Nieters, A. Ivan, S. Dolinsky, H. C. Climent, and A. M. Kasten, "Development of an electromagnetic imaging system for well bore integrity inspection," in *Proc. 43rd Annu. Rev. Prog. Quant. Nondestruct. Eval.*, Niskayuna, NY, USA, Feb. 2017, pp. 1–9.

[11] H. Guo, Z. Lv, Z. Wu, and B. Wei, "Multi-physics design of a novel turbine permanent magnet generator used for downhole high-pressure high-temperature environment," *IET Electr. Power Appl.*, vol. 7, no. 3, pp. 214–222, Mar. 2013.

[12] B. Dang, L. Yang, R. Dang, and Y. Xie, "Borehole electromagnetic induction system with noise cancelation for casing inspection," *IEICE Electron Express*, vol. 13, no. 17, pp. 1–9, Jul. 2016.

[13] B. Dang, L. Yang, C. Z. Liu, Y. H. Zheng, H. Li, R. Dang, and B. Q. Sun, "A uniform linear multi-coil array-based borehole transient electromagnetic system for non-destructive evaluations of downhole casings," *Sensors*, vol. 18, no. 8, pp. 1–16, Aug. 2018.

[14] C. Yang, B. Gao, Q. Ma, L. Xie, G. Y. Tian, and Y. Yin, "Multi-layer magnetic focusing sensor structure for pulsed remote field eddy current," *IEEE Sensors J.*, vol. 19, no. 7, pp. 2490–2499, Apr. 2019.
[15] Y. Fu, R. Yu, X. Peng, and S. Ren, "Investigation of casing inspection through tubing with pulsed eddy current," *Nondestruct. Test. Eval.*, vol. 27, no. 4, pp. 353–374, Dec. 2012.
[16] B. Dang, L. Yang, N. Du, C. Liu, R. Dang, B. Wang, and Y. Xie, "Auxiliary sensor-based borehole transient electromagnetic system for the nondestructive inspection of multipipe strings," *Sensors*, vol. 17, no. 8, pp. 1–15, Aug. 2017.
[17] H. M. Kim, H. R. Yoo, and G. S. Park, "Analysis of a defect signal deformations induced by eddy current in RFECT system for pipeline inspection," *IEEE Trans. Magn.*, vol. 54, no. 11, pp. 1–5, Nov. 2018.
[18] D. Voigt, J. L. W. A. Van Geel, and O. Kerkhof, "Spatio-temporal noise and drift in fiber optic distributed temperature sensing," *Meas. Sci. Technol.*, vol. 22, no. 8, pp. 1–8, Aug. 2011.
[19] L. Martin, J. Buchman, M. Bittar, R. Epstein, G. H. Hu, S. Zannoni, M. Morys, M. Rourke, and C. Platt, "Application of new asymmetrical array induction tool in hostile environments," in *Proc. 48th Annu. Logging Symp. SPWLA*, Austin, TX, USA, Jun. 2007, pp. 1–10.
[20] K. Behaimanot, M. Boeger, and A. Glasmachers, "Directional borehole radar antenna calibration," in *Proc. IEEE Instrum. Meas. Technol. Conf.*, Austin, TX, USA, Jun. 2010, pp. 1398–1403.
[21] X. Wu, G. Q. Xue, P. Xiao, J. T. Li, L. H. Liu, and G. Y. Fang, "The removal of the high-frequency motion-induced noise in helicopter-borne transient electromagnetic data based on wavelet neural networks," *Geophysics*, vol. 84, no. 1, pp. 1–37, Jan. 2019.
[22] Y. Ji, D. Li, M. Yu, Y. Wang, Q. Wu, and J. Lin, "A de-noising algorithm based on wavelet threshold-exponential adaptive window width-fitting for ground electrical source airborne transient electromagnetic signal," *J. Appl. Geophys.*, vol. 128, pp. 1–7, May 2016.
[23] X. Dai, L. Z. Cheng, J.-C. Mareschal, D. Lemire, and C. Liu, "New method for denoising borehole transient electromagnetic data with discrete wavelet transform," *J. Appl. Geophys.*, vol. 168, pp. 41–48, Sep. 2019.
[24] Y. Wang, Y. Ji, S. Li, J. Lin, F. Zhou, and G. Yang, "A wavelet-based baseline drift correction method for grounded electrical source airborne transient electromagnetic signals," *Explor. Geophys.*, vol. 44, no. 4, pp. 229–237, Dec. 2013.
[25] F. Liu, J. Li, L. Liu, L. Huang, and G. Fang, "Application of the EEMD method for distinction and suppression of motion-induced noise in grounded electrical source airborne TEM system," *J. Appl. Geophys.*, vol. 139, pp. 109–116, Apr. 2017.
[26] H.-P. Huang, S.-Y. Wei, H.-H. Chao, C. F. Hsu, L. Hsu, and S. Chi, "An investigation study on mode mixing separation in empirical mode decomposition," *IEEE Access*, vol. 7, pp. 100684–100691, Jul. 2019.
[27] H. Song, H. Dong, Z. Yuan, J. Zhu, H. Zhang, and Y. Huang, "An EEMD-based electromagnetic induction method for nondestructive testing of buried metal conductors," *IEEE Access*, vol. 7, pp. 142261–142271, Jul. 2019.
[28] M. Shamonin, A. Snarskii, and M. Zhenirovskyy, "Effective magnetic permeability of ferromagnetic composites. Theoretical description and comparison with experiment," *NDT E Int.*, vol. 37, no. 1, pp. 35–40, Jan. 2004.
[29] M. Blanco-Velasco, B. Weng, and K. E. Barner, "ECG signal denoising and baseline wander correction based on the empirical mode decomposition," *Comput. Biol. Med.*, vol. 38, no. 1, pp. 1–13, Jan. 2008.
[30] X. Lang, N. U. Rehman, Y. F. Zhang, X. Lei, and H. Y. Su, "Median ensemble empirical mode decomposition," *Signal Processing.*, vol. 176, pp. 1–8, Jun. 2020.
[31] X. Lang, Q. Zheng, Z. Zhang, S. Lu, L. Xie, A. Horch, and H. Su, "Fast multivariate empirical mode decomposition," *IEEE Access*, vol. 6, pp. 65521–65538, Sep. 2018.

BO DANG was born in Xi'an, China, in 1987. He received the Ph.D. degree in signal and information processing from Xidian University, in 2013. Since 2014, he has been taught with the Department of Electronic Engineering, Xi'an Shiyou University. He is an Assistant Professor with the Department of Electronic Engineering. His research interest includes downhole transient electromagnetic system for nondestructive testing and evaluation.

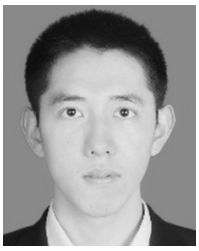

CHANGZAN LIU was born in Hebei, China, in 1989. He is currently pursuing the Ph.D. degree with the Information and Communication Engineering, Northwestern Polytechnical University, Xi'an, China. His research interest includes downhole transient electromagnetic system for reservoir exploration.

LING YANG was born in Shaanxi, China, in 1993. She is currently pursuing the Ph.D. degree with the Oil and Gas Engineering, Xi'an Shiyou University, Xi'an, China. Her research interest includes downhole transient electromagnetic oil and gas resource detection.

GANG WANG was born in Shaanxi, China, in 1996. He is currently pursuing the master's degree with the Measurement Technology and Instrument, Xi'an Shiyou University, Xi'an, China. His research interest includes transient electromagnetic annular array imaging detection technology for causing damage.

MIMI WANG was born in Shaanxi, China, in 1995. She is currently pursuing the master's degree with Precision Instrument and Mechanics, Xi'an. Her research interest includes defect inversion of the detection signals for downhole casings.

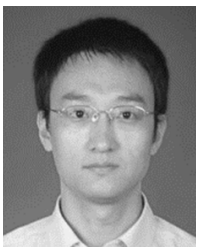

ZHIPING REN (Member, IEEE) was born in 1980. He received the Ph.D. degree from Chang'an University. He is currently an Associate Professor with the Department of Electronic Engineering, Xi'an Shiyou University, China. His research interests include nondestructive testing and evaluation of downhole casing.

RUIRONG DANG was born in 1957. He received the Ph.D. degree from the Nangjing University of Science and Technology, in 1991. He is currently a Professor with the Shaanxi Key Laboratory of Measurement and Control Technology for Oil and Gas Wells. Xi'an Shiyou University, China. His current research interests include intelligent well layered measurement and control systems.